Results in Physics 61 (2024) 107759

Contents lists available at ScienceDirect

Results in Physics

journal homepage: www.elsevier.com/locate/rinp

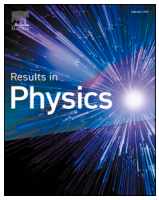

Gamma alumina as a saturable absorbing material for C- and L-band ultrafast mode-locked fiber lasers

N.F. Pikau [a], N. Mohd Yusoff [b,c,*], A.R. Sarmani [a], F.D. Muhammad [a], M.T. Alresheedi [d], E.K. Ng [e], M.A. Mahdi [b,f,**]

[a] Department of Physics, Faculty of Science, Universiti Putra Malaysia, 43400 Serdang, Selangor, Malaysia
[b] Institute of Nanoscience and Nanotechnology (ION2), Universiti Putra Malaysia, 43400 Serdang, Selangor, Malaysia
[c] inLAZER Dynamics Sdn. Bhd., InnoHub Unit, Putra Science Park, Universiti Putra Malaysia, 43400 Serdang, Selangor, Malaysia
[d] Department of Electrical Engineering, College of Engineering, King Saud University, P.O. Box 800, Riyadh 11421, Kingdom of Saudi Arabia
[e] Department of Engineering, University of Cambridge, Cambridge CB3 0FA, United Kingdom
[f] Wireless and Photonic Networks Research Centre, Faculty of Engineering, Universiti Putra Malaysia, 43400 UPM Serdang, Selangor, Malaysia

ARTICLE INFO

Keywords
Mode-locked
Gamma-alumina
Saturable absorber
Erbium-doped fiber laser

ABSTRACT

This work demonstrates femtosecond pulse generations in C- and L-band regimes utilizing a gamma-aluminum oxide/polydimethylsiloxane saturable absorber (γ-Al_2O_3/PDMS-SA) via mode-locking technique. The γ-Al_2O_3/PDMS-SA has a 7.3% modulation depth and a moderate saturation intensity of 303 MW/cm^2, and estimated damage threshold of greater than 8.49 and 3.57 GW/cm^2 pumping intensities in C- and L-band wavelengths, respectively. In the C-band laser cavity, the generated mode-locked pulse delivered a low threshold of 28.7 mW and an ultrafast width of 622 fs. Meanwhile, a higher threshold of 108.6 mW and 942 fs pulse width were measured in the L-band laser cavity centered at 1611 nm. These demonstrations showcase a versatile feature of γ-Al_2O_3 as a light-absorbing material that generates ultrashort pulses in a wideband wavelength range, which could benefit future research on the metastable state of aluminum-based materials within the field of ultrafast photonics.

Introduction

Pulsed lasers, especially in the generation of ultrashort width in femtosecond ranges, became the focus of research after the development of the first fiber laser in 1980, and currently received a great deal of interest to fulfill the industry demands on bone tissue ablation [1], high precision micromachining for material processing [2], photonic-chip device [3] and flexible sensor [4] fabrications. These pulses can be generated using a mode-locking technique, in which the cavity longitudinal modes are locked together through active and passive techniques. The former approach is made possible by using a modulator, such as an electro-optic modulator that modulates the resonator losses to produce pulses [5]. This technique is fast, typically in nanoseconds and adjustable, but it has limitations such as bulky components and is expensive. Meanwhile, the latter technique uses a bleached saturable absorber (SA) by employing its nonlinear absorption characteristics to initiate the optical pulse. Semiconductor saturable absorber mirrors (SESAMs) [6], graphene [7] and carbon nanotubes [8], black phosphorus [9], and MXene [10] have been most extensively explored for their excellent features of SA and the ultrashort pulse generations. Recently, metal oxides such as ferroferric-oxide (Fe_3O_4) [11], zinc oxide (ZnO) [12], and magnesium oxide (MgO) [13] have attracted much attention as SA due to their high nonlinear optical absorption ranges from visible to mid-infrared wavelengths, fast recovery time and excellent mechanical strength [11–13].

Aluminum oxide (Al_2O_3), is another metal oxide known as polymorphic materials present themselves in stable α-phase and various metastable phases of crystalline structure [14]. The material's durability under extreme conditions is evidenced from its demand in ceramics manufacturing [15,16], and served as a coating layer for improving thermal tolerance of metal's surface [17]. One of metastable phase, namely gamma alumina (γ-Al_2O_3) possess a great deal of interest in

* Corresponding author at: Institute of Nanoscience and Nanotechnology (ION2), Universiti Putra Malaysia, 43400 Serdang, Selangor, Malaysia.
** Corresponding author at: Wireless and Photonic Networks Research Centre, Faculty of Engineering, Universiti Putra Malaysia, 43400 UPM Serdang, Selangor, Malaysia
E-mail addresses: noritayusoff94@gmail.com (N. Mohd Yusoff), mam@upm.edu.my (M.A. Mahdi).

https://doi.org/10.1016/j.rinp.2024.107759
Received 6 March 2024; Received in revised form 5 May 2024; Accepted 11 May 2024
Available online 13 May 2024

heterogenous catalysis due to its acidic feature and large surface area [18]. Furthermore, the adsorbing ability of γ-Al_2O_3 for arsenic removal has been demonstrated to prove that this material has superior adherence towards hazardous element [19]. Aside from that, γ-Al_2O_3 possess saturable absorbing characteristics, by having nonlinear refractive index of 3.67 × 10^{-8} cm^2/W and nonlinear absorption coefficient of 6.6 × 10^{-4} cm/W, respectively, determined from a z-scan method [14]. To this end, the researches on Al_2O_3 in pulsed fiber lasers are limited to α-phase crystal structure for the generation of single wavelength [20,21], dual-wavelength [22], and tunable wavelength [23] of Q-switched pulses. This approach manipulates the intracavity loss and deliver microsecond width of optical pulses. Meanwhile, the mode-locked pulse co-existed in Q-switched envelope [24] and double-scale temporal profile of noise-like pulse [25] have been reported thereafter. Therefore, there is always a research opportunity to explore other phase of Al_2O_3 families for ultrashort pulse generation of less than picoseconds regime.

In this paper, γ-Al_2O_3 was blended with the polydimethylsiloxane (PDMS) as a binding agent, then coated onto a tapered fiber to form a reliable γ-Al_2O_3/PDMS-SA. The SA was inserted into ring configuration of erbium-doped fiber lasers operating in C- and L-band regimes for femtosecond pulse generations. Under the C-band operation, a pulse width of 622 fs was obtained at 1560.86 nm central wavelength. By changing the erbium-doped fiber (EDF), the ultrashort pulse was achieved in the L-band regime at 1610.94 nm central wavelength with 942 fs pulse width. The fabricated SA based on a tapered fiber has a high damage threshold, providing an alternative for high-power operation with estimated damage threshold of larger than 8.49 GW/cm^2 and 3.57 GW/cm^2 input intensities for C- and L-band operations, respectively. These findings open infinite possibilities for future advancement of metastable state of aluminum-based materials within the field of ultrafast photonics.

γ-Al_2O_3/PDMS-SA fabrication and characterizations

The methodology of preparing γ-Al_2O_3/PDMS composite is presented in Fig. 1. The γ-Al_2O_3 powders were commercially available from ACS Material, LLC, USA (8–12 nm, 99%) and were directly used without further purification. The homogenous solution of γ-Al_2O_3 was prepared by dispersing 2 mg of γ-Al_2O_3 powders in 10 mL of isopropyl alcohol (IPA, 99.5%, Sigma Aldrich). The γ-Al_2O_3/IPA mixture was then sonicated using an ultrasonic equipment (Hielscher UP200s) with an amplitude of 100% and a cycle of 0.5 within 2 h. After that, the solution was mixed with 1 g of PDMS (Sylgard®184 silicone elastomer, purchased from Dow Corning). The solution was heated afterwards under a stirring condition at 80 °C on a magnetic hotplate. Aside from that, an adiabatic tapered fiber with dimensions of 30 mm transition length, 0.8 mm waist length, and 10 μm waist diameter was fabricated using a Vytran GPX-3400 optical processing workstation. The optical fiber used was single mode fiber (Corning SMF-28), heated at 50 W filament power and stretched according to the desired parameters as previously mentioned. Then, the fabricated tapered fiber was transferred on a flat substrate and ready for the next step of material deposition. Following that, a polymer hardener (0.1 g) was added into the as-prepared composite material and continuously stirred for 10 min. The viscous γ-Al_2O_3/PDMS composite was treated in a vacuum condition for the process of air-bubble removal for 30 min. The final composite was

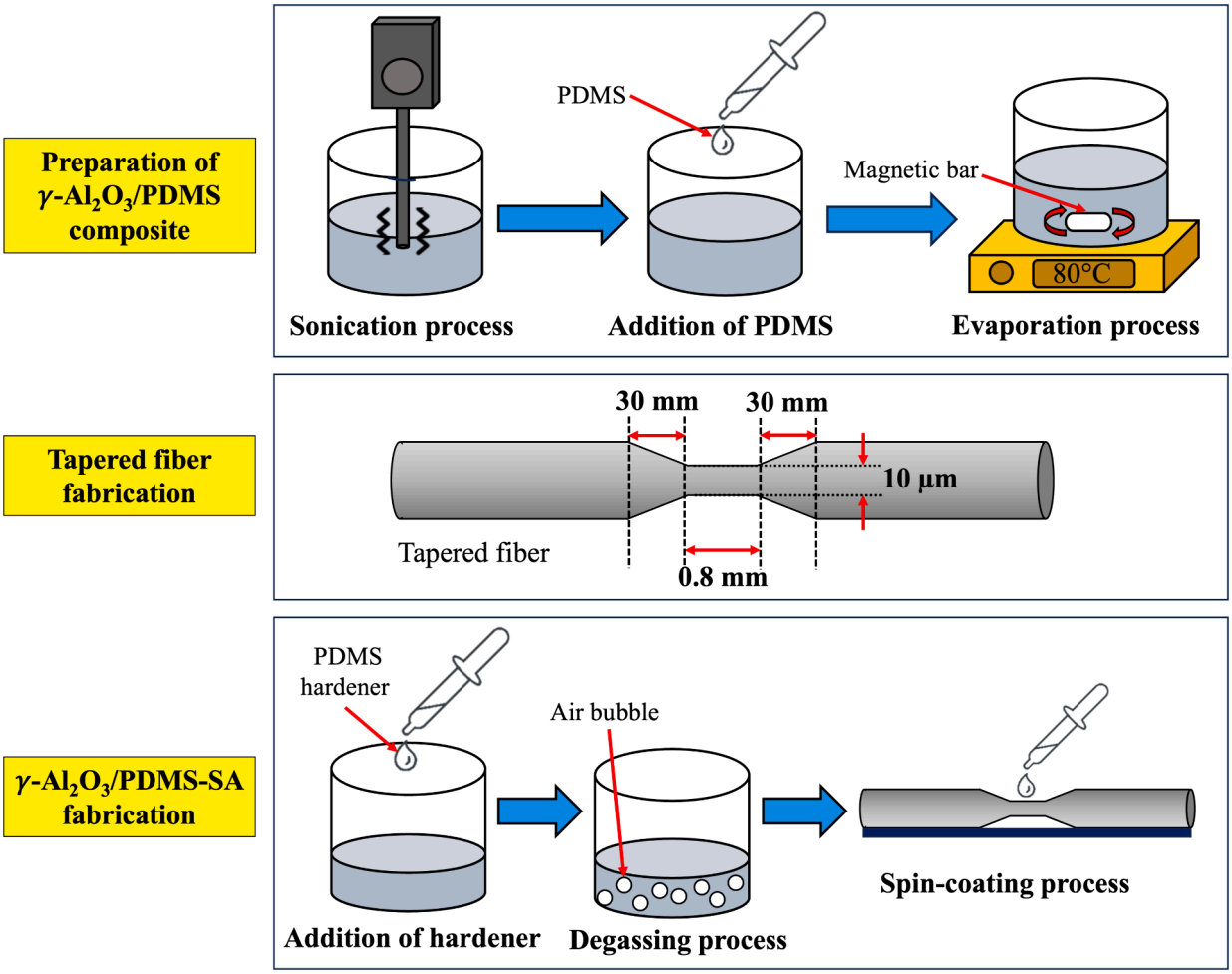

Fig. 1. The methodology of γ-Al_2O_3/PDMS-SA fabrication.

dropped on the tapered fiber region, followed by spin-coating procedure at 4000 rotation per minute with a duration of 5 min. Finally, the fabricated γ-Al_2O_3/PDMS-SA was hardened in a laboratory environment for 2 days.

Fig. 2 presents the characterization of γ-Al_2O_3 powders. The field emission scanning electron microscope (FESEM) image is illustrated in Fig. 2(a), characterized using a FEI Nova NanoSEM 230 with accelerating voltage of 18 kV. The micrograph shows that γ-Al_2O_3 powders existed in an agglomerate cluster, whereas its elemental compositions are displayed in Fig. 2(b). The elemental dispersive X-ray (EDX) analysis shows high purity of sample; evidenced from the inset of Fig. 2(b); 51.20% of oxygen (O) and 48.80% of aluminum (Al) elements with no detection of other foreign elements. Fig. 2(c) shows the X-ray diffraction (XRD) spectrum of γ-Al_2O_3, the characterization was performed using a Rigaku SmartLab (Cu-$K\alpha$ radiation wavelength of 1.5406 Å). All the XRD peaks are indexed according to the database JACDS Card No: 80–1385, reflected to a cubic crystallographic system with a lattice parameter, a = 7.9382 Å [26]. From Fig. 2(c), the identified peaks at 19.56°, 32.86°, 37.50°, 39.32°, 45.65°, 60.86°, and 67.02° are corresponded to (111), (220), (311), (222), (400), (511), and (440) planes, respectively. Referring to the most intense peak at 2θ = 67.02°, the d-spacing and crystallite size are determined to be 1.3953 Å and 8.9 nm, correspondingly. The values obtained are reflected from the hkl plane of (440), calculated using Scherrer's equation. On the other hand, ultraviolet–visible-near-infrared spectroscopy (UV–Vis-NIR, Shimadzu UV-3600) was performed to characterize the absorbance of γ-Al_2O_3 powders. Fig. 2(d) shows the absorption spectrum covering from UV to NIR regions, which proposes the applicability of γ-Al_2O_3 in photonics applications such as SA.

Next, the optical characterizations of γ-Al_2O_3/PDMS-SA were carried out which are represented in Fig. 3. The transmission loss γ-Al_2O_3/PDMS-SA was determined from an experimental setup consisted of a light source and an optical spectrum analyzer (OSA, Yokogawa AQ6370B), schematically presented in Fig. 3(a). The measured loss of γ-Al_2O_3/PDMS-SA was 4.7 and 4.5 dB at 1.56 and 1.61 μm, correspondingly. In addition to that, the nonlinear transmission of γ-Al_2O_3/PDMS-SA was evaluated via a twin-balanced detector measurement as depicted in the Fig. 3(c). The setup is comprised of a femtosecond pulse laser source operating at 1560 nm, 150 fs pulse width, and 60 MHz repetition rate. The adjustment of optical power was done by a manual attenuator, and an isolator was utilized to block any back-reflected power into the pulse source. The splitting power with equivalent ratio of 50% was made possible by incorporating a 50/50 optical coupler (OC), whereas both output ports were connected to optical power meters for qualitative data collection. The nonlinear transmission curve is portrayed in Fig. 3(d), whereby the experimental data was fitted according to the following expression;

$$T(I) = 1 - \Delta T\left[exp\left(-\frac{I}{I_{sat}}\right)\right] - T_{ns}$$

The modulation depth (ΔT) was identified to be 7.3%, which is higher than the previous work (3.5%) reported by Al-Hayali et al. [20], and comparable to Al-nanoparticles-SA (7%) [27] as well as α-Al_2O_3-SA (6.24%) [24]. The incident intensity acquired to saturate the half of the SA's modulation depth, defined as saturation intensity (I_{sat}) was estimated to be 303 MW/cm^2. Aside from that, the non-saturable loss (T_{ns}) resulted from the accumulated effects of unavoidable scattering effect at the tapered region, material/polymer concentration, imperfection of substrate fabrication was measured to be 63%, considerably matched with the loss profile in Fig. 3(b).

Integration of γ-Al_2O_3/PDMS-SA into an erbium-doped fiber laser cavity

Fig. 4 portrays the schematic layout of an erbium-doped fiber laser (EDFL) which incorporates γ-Al_2O_3/PDMS-SA as a pulse initiator. A 980 nm laser diode (LD) was utilized to allow erbium ions excitation in an active gain medium with an 8 m long length (EDF, model Lucent HP980). The low concentration EDF with an absorption of 4 dB/m at 1530 nm ensured the operational wavelength within the C-band region. The photons supplied from the 980 nm LD into the gain medium were made possible by incorporating an optical component called a

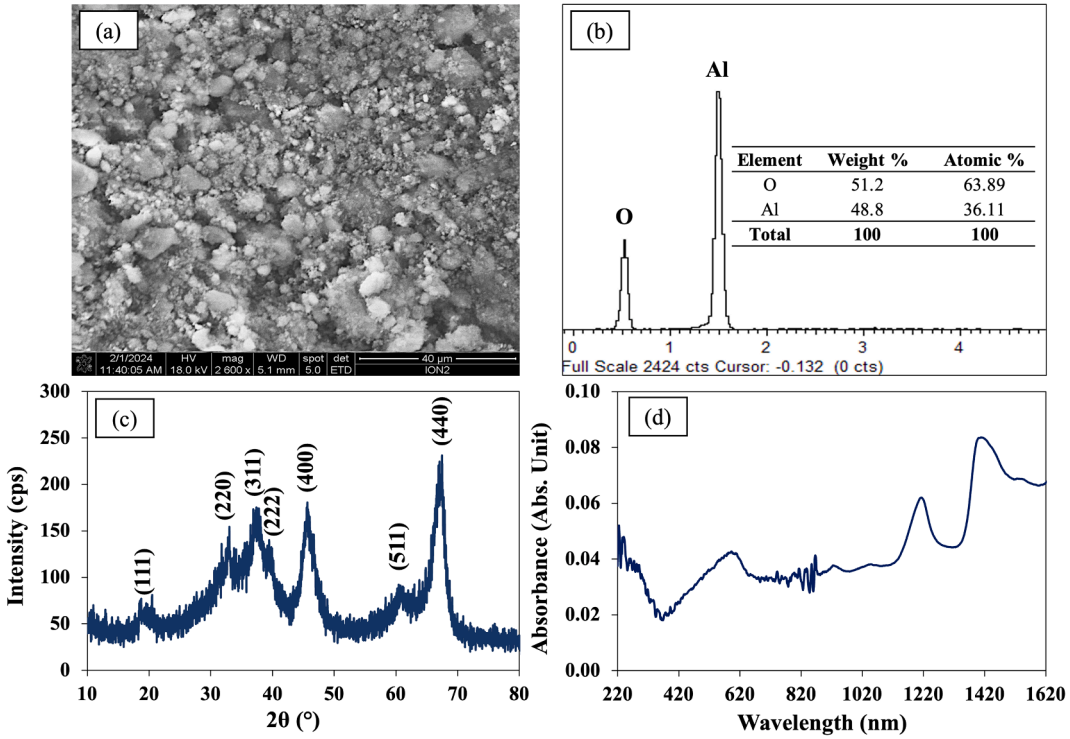

Fig. 2. Characterizations of the γ-Al_2O_3 powders, (a) The FESEM image, (b) EDX spectrum, and (d) UV–Vis-NIR absorption profile.

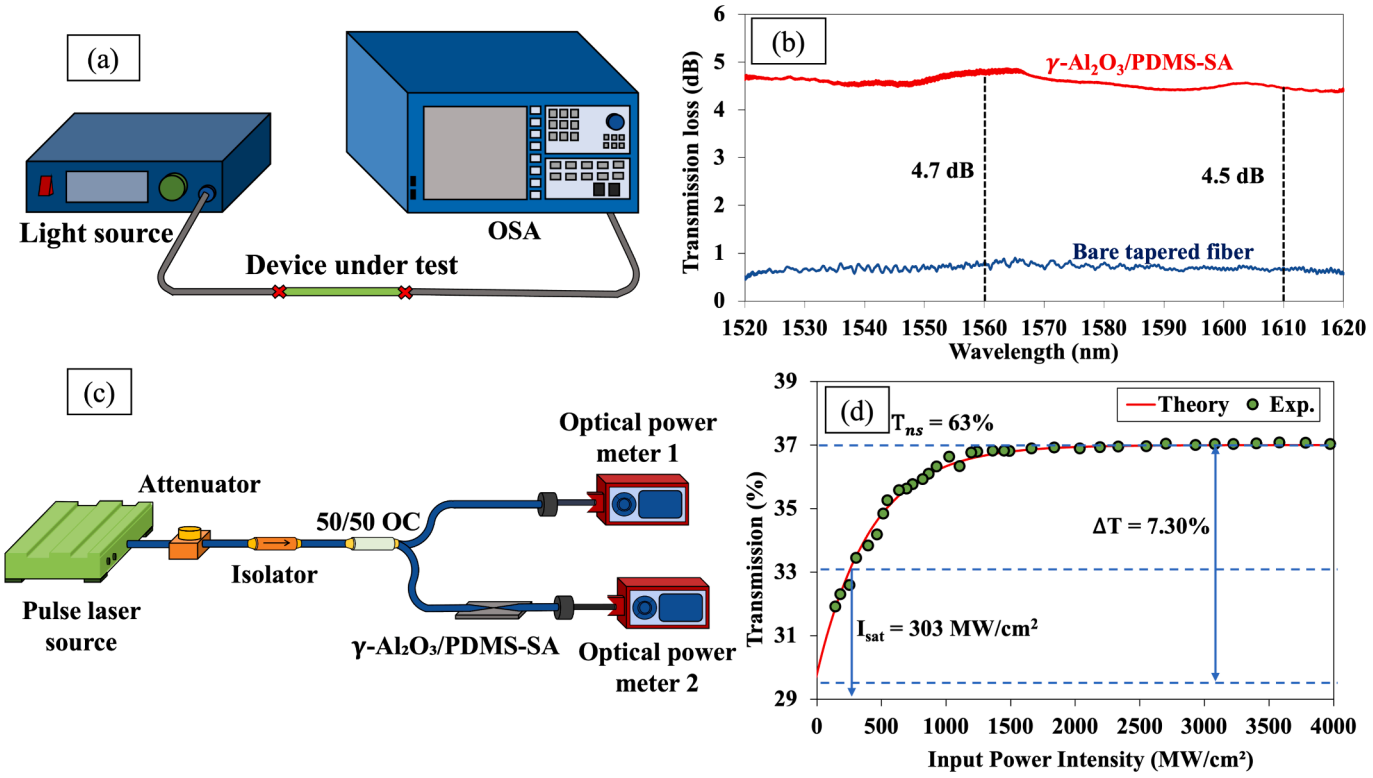

Fig. 3. Optical characterizations of γ-Al_2O_3/PDMS-SA; (a) experimental setup of loss characterization, (b) the transmission loss profile, (b) the experimental setup of twin-balanced detector setup, and (c) the nonlinear transmission curve γ-Al_2O_3/PDMS-SA.

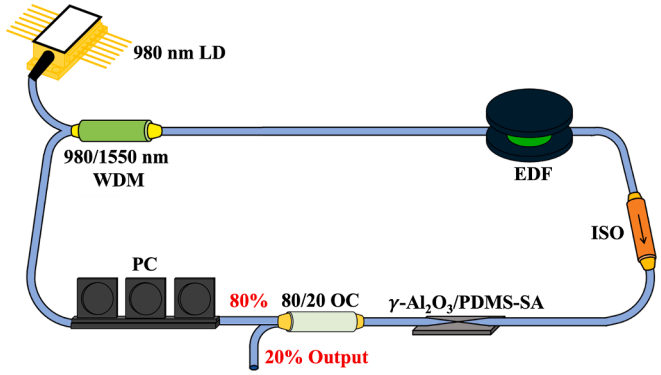

Fig. 4. Experimental setup of the EDFL based on γ-Al_2O_3/PDMS-SA.

wavelength division multiplexer (WDM) that covers both the pump and signal wavelengths of 980/1550 nm. A polarization-insensitive isolator (ISO) was added to force the light oscillations in one direction. Thereafter, the γ-Al_2O_3/PDMS-SA was inserted following the amplifying section, whereas a piece of OC with a splitting ratio of 80/20 was utilized to divide the optical signal into two different directions; the large power ratio was directed to the amplifying section of the laser resonator through a three-paddle polarization controller. Meanwhile, the small power ratio was connected to the equipment for pulse performance evaluations, data collection and analysis, and troubleshooting purposes. The equipment used in the experiment were an optical spectrum analyzer (OSA, Yokogawa AQ6370B), an oscilloscope (Tektronix TDS 3012C), an electrical spectrum analyzer (GW Instek GSP-830), an autocorrelator (APE PulseCheck 150), and an optical power meter (OPM, Thorlabs PM100D and S148C thermal sensor).

In the L-band laser cavity, the optical components arrangement was maintained, while the previous mentioned EDF in the C-band laser configuration was changed to a new EDF with 7 m length (Liekki Er80-4/125). It is known that the L-band has a lower gain coefficient in contrast to the C-band. Incorporating the highly-doped EDF with 80 dB/m absorption at 1530 nm facilitated the laser emission in the L-band region. An additional SMF-28 of 11 m length was added into the L-band laser cavity, mainly to optimize the laser cavity dispersion and stabilize the pulse output. The total cavity length for C- and L-bands were 20.2 m and 31.8 m, respectively. The dispersion coefficient (β_2) and group velocity dispersion (GVD) for each fiber in the C- and L-bands laser cavities are summarized in Table 1.

The net GVD for C- and L-bands were approximated to be −0.0694 and −0.296 ps^2, respectively, affirming net anomalous dispersion characteristics of laser cavities.

Results

C-band mode-locked operation

In this experiment, there was no mode-locking operated in the laser cavity without the presence of γ-Al_2O_3/PDMS-SA. Upon the placement of the γ-Al_2O_3/PDMS-SA into the C-band laser cavity, a narrow

Table 1
Calculation of net GVD for each optical fiber used in C- and L-band setups.

Laser cavity	Fiber type	Length (m)	β_2(ps^2/km)	Net GVD (ps^2)
C-band	SMF-28	11.2	−22.0	−0.246
	Hi-1060	1.0	−7.0	−0.007
	EDF	8.0	+23.0	+0.184
	Total	20.2		−0.0694
L-band	SMF-28	23.8	−22.0	−0.524
	Hi-1060	1.0	−7.0	−0.007
	EDF	7.0	+33.6	+0.235
	Total	31.8		−0.296

linewidth of continuous-wave (CW) laser emission was firstly observed at 13.8 mW, and emerged to a mode-locked operation at 28.7 mW pump power as presented in Fig. 5(a). The appearance of Kelly sidebands in the optical domain validated anomalous dispersion operational laser cavity in the C-band region. At 260 mW pump power, the soliton optical spectrum centered at 1560.86 nm with 5.21 nm spectral bandwidth, as displayed in a green line of Fig. 5(a).

In Fig. 5(b), the generated pulse portrayed a full width at half maximum (FWHM) of 0.96 ps, reflecting a $sech^2$ shape profile of 622 fs. From these pulse properties, the time bandwidth product (TBP) was determined to be 0.398. As the transform limited soliton pulse of $sech^2$ profile has the TBP value of 0.315, the obtained pulse in the C-band regime was determined to be slightly chirped. Fig. 5(c) illustrates a well-defined mode-locked pulses with 95 ns spacing, representing 20.2 m cavity length and 10.47 MHz repetition rate. Besides that, the RF spectrum shown in Fig. 5(d) exhibits a signal-to-noise ratio (SNR) of 58.9 dB at the fundamental repetition rate, while no abnormalities were detected across 100 MHz frequency span. Aside from that, the linear progression of output power and pulse energy are summarized in Fig. 6, whereby up to 11.23 mW and 1.07 nJ were attained at 260.0 mW pump power.

The output spectrum and autocorrelation trace were recorded every 3 min for a duration of 200 min are demonstrated in Fig. 7. Besides that, the 3-dB bandwidth, central wavelength, pulse width and TBP that correspond to the recorded data are compiled in Fig. 9(b) and (d), respectively. There were no significant changes of spectra or any shifts recorded in both optical and temporal domains. The average values of 3-dB bandwidth, central wavelength, TBP and pulse width were 5.24 ± 0.03 nm, 1560.84 ± 0.01 nm, 0.403 ± 0.003 and 624 ± 1 fs, correspondingly. The small deviations affirmed a good stability of C-band operation with γ-Al_2O_3/PDMS-SA.

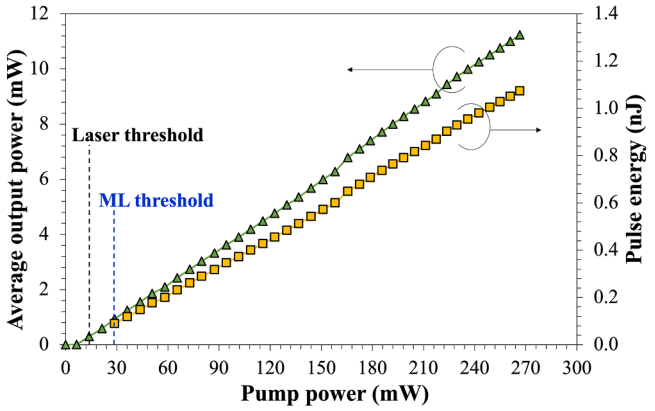

Fig. 6. Output power and pulse energy against the pump power of C-band mode-locked fiber laser.

L-band mode-locked operation

For an L-band laser scheme, the first emission of CW regime was observed when the 980 nm LD was set at 72.8 mW. By increasing the pump power to 108.6 mW, the initial soliton pulse emission with Kelly sidebands was recorded as depicted in Fig. 8(a). At 260.0 mW pump power, the measured central wavelength and spectral bandwidth were 1610.94 and 4.11 nm, respectively. Meanwhile, the generated pulse plotted in Fig. 8(b) had 1.454 ps FWHM, and real pulse width was calculated to be 942 fs, assuming a $sech^2$ pulse profile. Therefore, the TBP was calculated to be 0.45, significantly higher degree of chirping

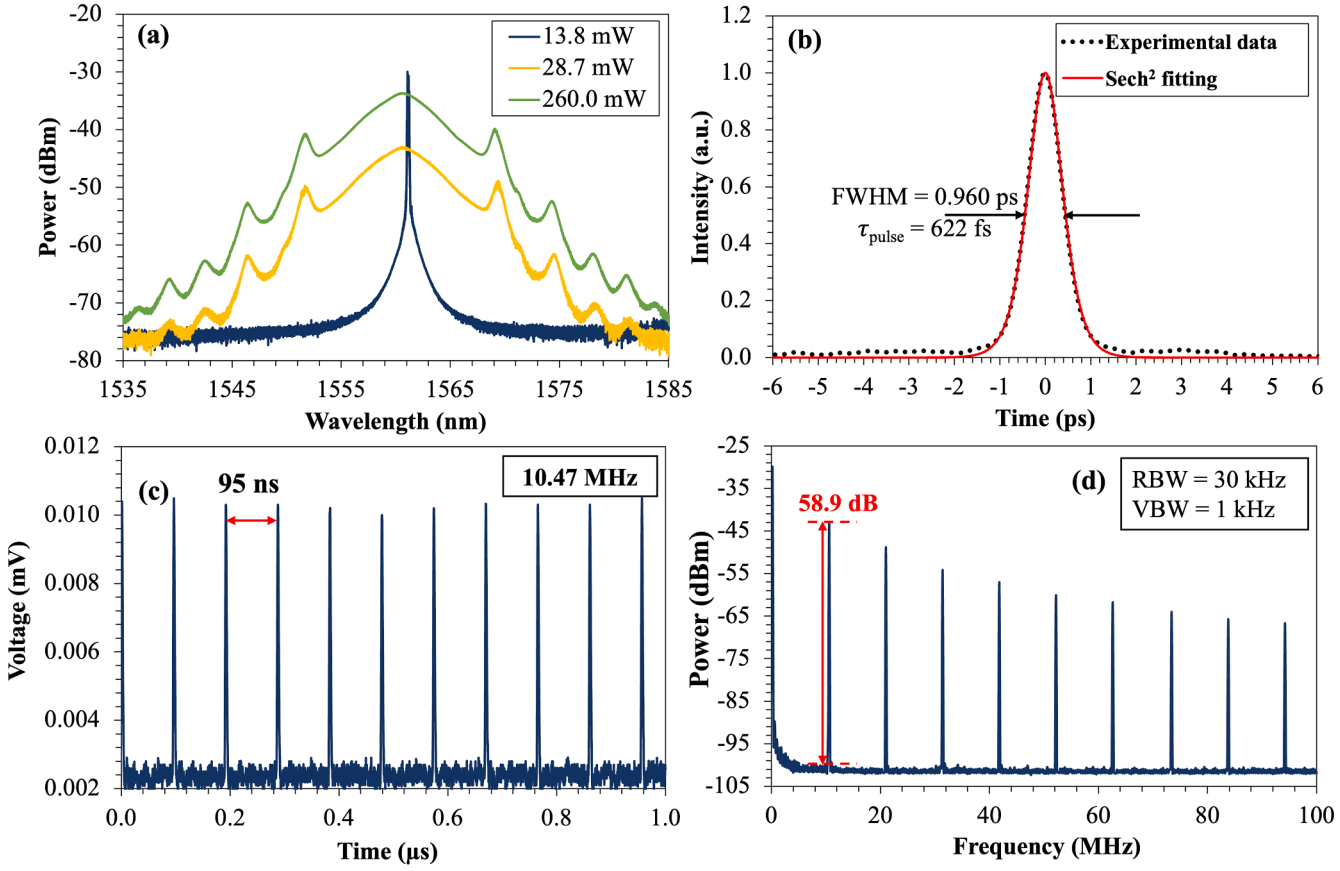

Fig. 5. Characteristics of C-band mode-locked fiber laser, (a) optical spectra at different pump powers, (b) autocorrelation trace, (c) oscilloscope trace, and (d) RF spectrum.

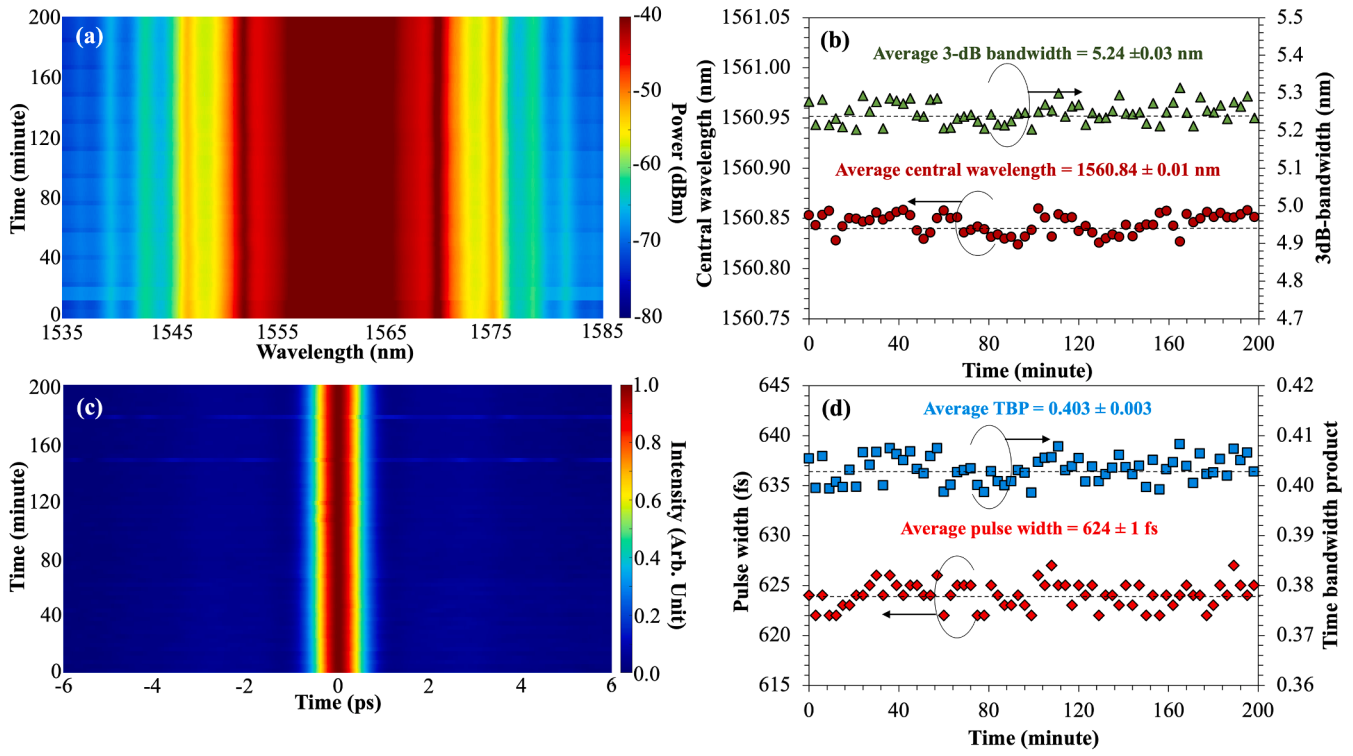

Fig. 7. Stability evaluation of C-band mode-locked fiber laser over 200 min, (a) optical spectra, (b) 3-dB bandwidth and central wavelength, (c) autocorrelation traces, and (d) TBP and pulse width.

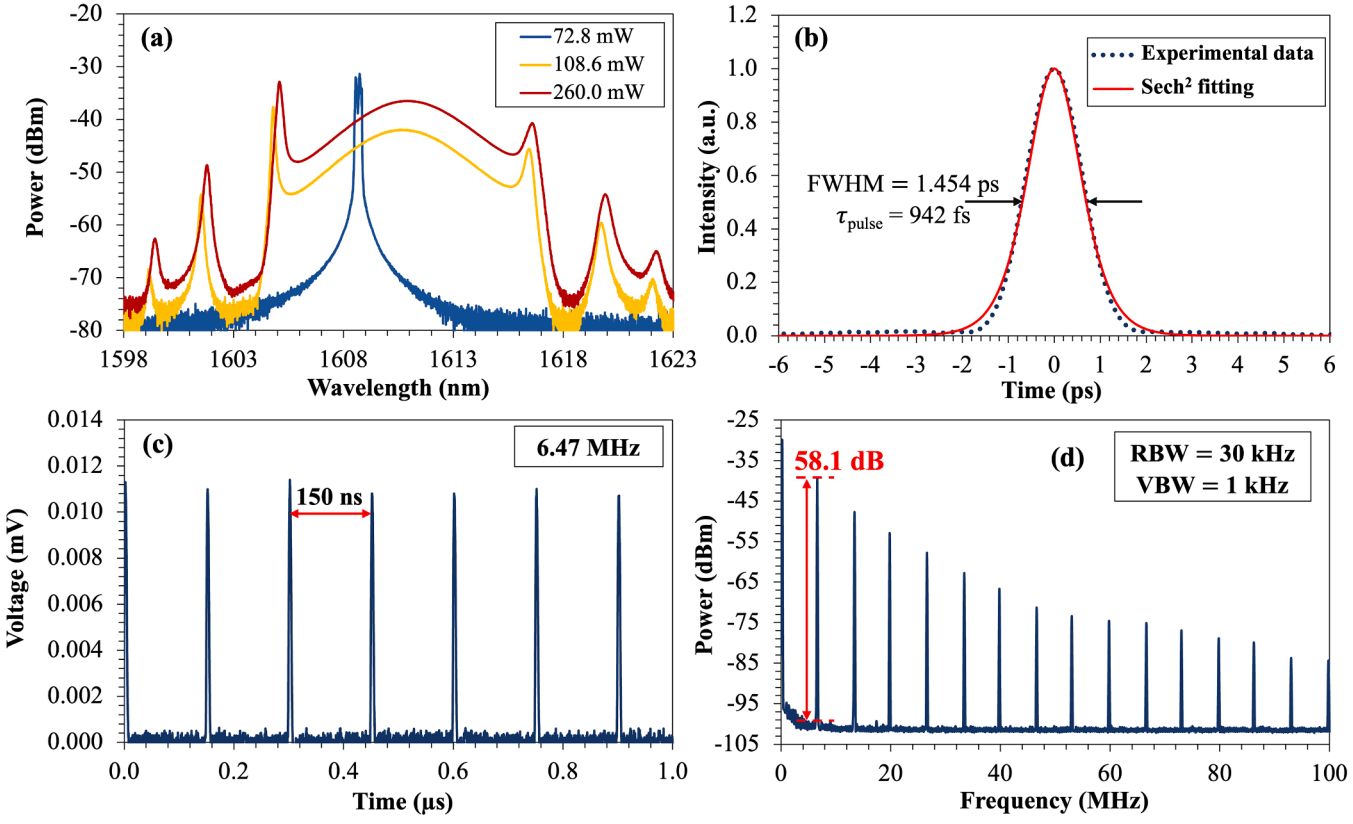

Fig. 8. Characteristics of L-band mode-locked fiber laser, (a) optical spectra at different pump powers, (b) autocorrelation trace, (c) oscilloscope trace, and (d) RF spectrum.

compared to its C-band pulse counterpart. Fig. 8(c) depicts the pulse train of 150 ns round-trip time, which is related to 6.47 MHz repetition rate and 31.8 m cavity length. The RF trace was captured for 100 MHz frequency span, as plotted in Fig. 8(d). At 6.47 MHz repetition rate, the result showed 58.10 dB SNR, implying a considerable stable operation of generated mode-locked pulse in the L-band fiber laser cavity. Besides that, the output power and pulse energy reached 4.65 mW and 0.71 nJ, respectively, at maximum pump power as shown in Fig. 9.

The stability assessment of L-band mode-locked operation was performed using similar procedure conducted in the C-band operation previously. The spectral outputs over 200 min are presented in Fig. 10 (a), whereas the analyses plotted in Fig. 10(b) revealed the central wavelength of 1610.28 ± 0.01 nm and spectral bandwidth of 3.80 ± 0.01 nm. On the other hand, autocorrelation traces of $sech^2$ pulse profile are depicted in Fig. 10(c), having insignificant drift in pulse width and TBP with the values of 955 ± 2 fs and 0.420 ± 0.002, respectively. Therefore, from these observations, it can be concluded that the L-band mode-locked operation had stable operation throughout the experiment.

Discussion

Table 2 summarizes past works of metal oxides functioned as SA material for ultrashort pulse generation in the region of C-band wavelengths. Besides the material's capability of absorbing light, the main factor that influences the nonlinear properties of SA is fabrication method; namely, SA template used, the embedding procedure of material onto SA template of either with or without polymer matrix, and concentration of material in polymer matrix. A sandwich-type based fiber ferrule approach of material/polymer composite is very popular in the past [28–33]. To prepare the SA using this route, several polymers were previously incorporated, namely polyethylene glycol (PEG) [34], polyethylene oxide (PEO) [28,32] and polyvinyl alcohol (PVA) [29–33]. For instance, Sadeq et al. [29] fabricated 20 μm thickness of copper oxide (CuO)/PVA composite from a mass ratio of 5 mg CuO: 1 g PVA, demonstrating the SA with 3.5% ΔT. Increasing the thickness and material's concentration in polymer matrix, higher ΔT of 13.0% was achieved by Co_3O_4/PVA-SA [30]. By utilizing an identical mass ratio of material and polymer (50 mg: 1 g), Y_2O_3/PVA-SA had higher ΔT (38.0%) [33] over Lu_2O_3/PVA-SA (10.0%) [31]. Guided by the non-saturable loss of both SAs, Y_2O_3 is stipulated to have higher absorbing property in the NIR region as compared to Lu_2O_3. Meanwhile, up to 39.0% ΔT was attained with 180 μm thickness by nickel oxide (NiO)/PEO-SA [32]. However, it must be emphasized that both aforementioned factors need to be carefully adjusted to avoid high T_{ns} of the SA, which negatively impact the overall performance of the fiber laser system. This circumstance was also applicable for the polymer composite-based tapered fiber SA, as reported in Ref. [35] and this work.

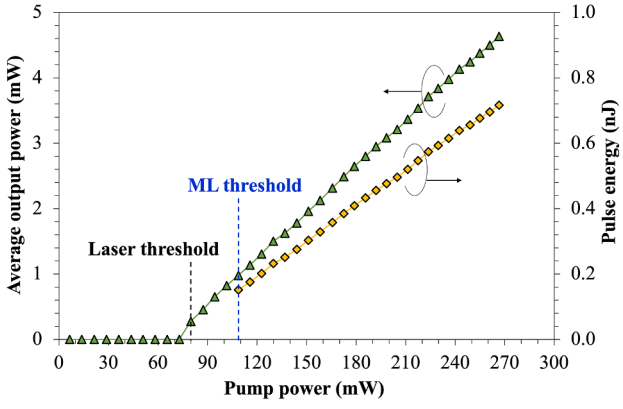

Fig. 9. Output power and pulse energy against the pump power of L-band mode-locked fiber laser.

Aside from that, the direct materials deposition onto SA templates have also been investigated; namely drop-casting, optical deposition, and magnetron sputtering techniques. As the material attachment of drop-casting method is in a random manner, the reproducibility of this method is rather challenging. This is evidenced from the work reported by Wang et al., in which vanadium dioxide (VO_2) solution was dropped casted onto a D-shaped fiber with the lowest ΔT of 3.0% [36]. In addition to that, the low ΔT was also influenced by the remaining depth of the polished region of D-shaped fiber [36]. Inversely, the optical deposition and magnetron sputtering methods offer alternatives to increase the success rate of the SA fabrication and improved the SA properties. These are well-demonstrated by the optically deposited methylene blue loaded reduced titanium dioxide (TiO_{2-x}-MB) and magnetron-sputtered chromium oxide (Cr_2O_3) onto tapered fibers with measured ΔT of 7.1% [37] and 12.5% [38], respectively. Overall, the measured ΔT of the γ-Al_2O_3/PDMS-SA was 7.3%, which was comparable to Ref. [28,37], larger than Ref. [29,35,36], and smaller than Ref. [30–33,38]. Meanwhile, our γ-Al_2O_3/PDMS-SA permitted significantly large T_{ns} except in Ref. [30,38].

The critical pulse properties such as mode-locked threshold power, pulse width, output power, repetition rate and pulse energy are also dependent on the laser cavity parameters. In the C-band laser operation, an ultrashort pulse of 334 fs was recorded by Cr_2O_3-SA, achieved by the shortest cavity length that corresponded to 34.48 MHz repetition rate [38]. By using a slightly longer cavity length with 22.91 MHz repetition rate, Wang et al. observed slow pulse width of 1.29 ps with their D-shaped fiber based VO_2-SA [36]. In addition to that, the asymmetrical architecture of this SA negatively impacted the pulse performances due to its susceptibility towards different polarization angles. Therefore, a deliberate adjustment of PC was necessary to start the mode-locked operation as the fabricated VO_2-SA was unable to self-start. Besides that, a fair comparison can be made between this work and NiO/PDMS-SA [35] due to its comparable T_{ns}. Aziz et al. [35] extracted higher percentage of intracavity power for analysis as compared to this work (30% vs. 20%). Therefore, slightly higher pump power is required to compensate the intracavity loss and achieve mode-locked operation in Ref. [35]. This is also resulted in lower output power of 7.14 mW in Ref. [35] as compared to this work (11.23 mW). Aside from that, although vanadium pentoxide (V_2O_5)/PEO-SA possess lower T_{ns} as compared to our γ-Al_2O_3/PDMS-SA, Nady et al. observed the mode-locked operation at significantly higher pump power (80.0 mW) due to the longer length of the laser cavity [28]. Nevertheless, the low repetition rate of 1.0 MHz cavity accumulated intracavity pulse energy, which well-translated to 4.44 nJ output pulse energy extracted from 20% output coupler [28]. This approach also had been practiced in several other works [29,31–33]. From the literatures in Table 2, the highest pulse energy of 25.80 nJ was achieved by Y_2O_3/PVA-SA at the expense of slowest pulse width of 4150 fs [33]. Overall, this work demonstrated the lowest mode-locking threshold and an ultrafast pulse width as opposed to other works [28–33,35–38], highest output power of 11.23 mW, which is comparable to Ref. [30], and slightly lower than Ref. [33], as well as moderate pulse energy of 1.07 nJ operating in the C-band region.

Table 3 tabulates the reported works on metal oxides as a SA generating L-band soliton pulse centered in between 1565.40 to 1610.94 nm wavelengths. The ZnO/PVA-SA in Ref. [39] was reported to initiate mode-locked operation at very low pump power of 42.0 mW. The switching mode from continuous to mode-locked pulse regime is mainly ascribed by the intracavity pulse energy. However, the stable mode-locked operation was limited to 159 mW pump power, as it became unstable beyond this power level [39]. Other than that, Wang et al. reported that the Fe_3O_4 deposited tilted fiber grating (TFG)-SA in the L-band cavity experienced pulse splitting effect beyond 200 mW pump power [41]. Meanwhile, the mode-locked operations demonstrated by holmium oxide (H_2O_3)/PVA-SA [40] and V_2O_5/PEG-SA [34] were reverted back to CW emissions beyond 180 mW and 107 mW,

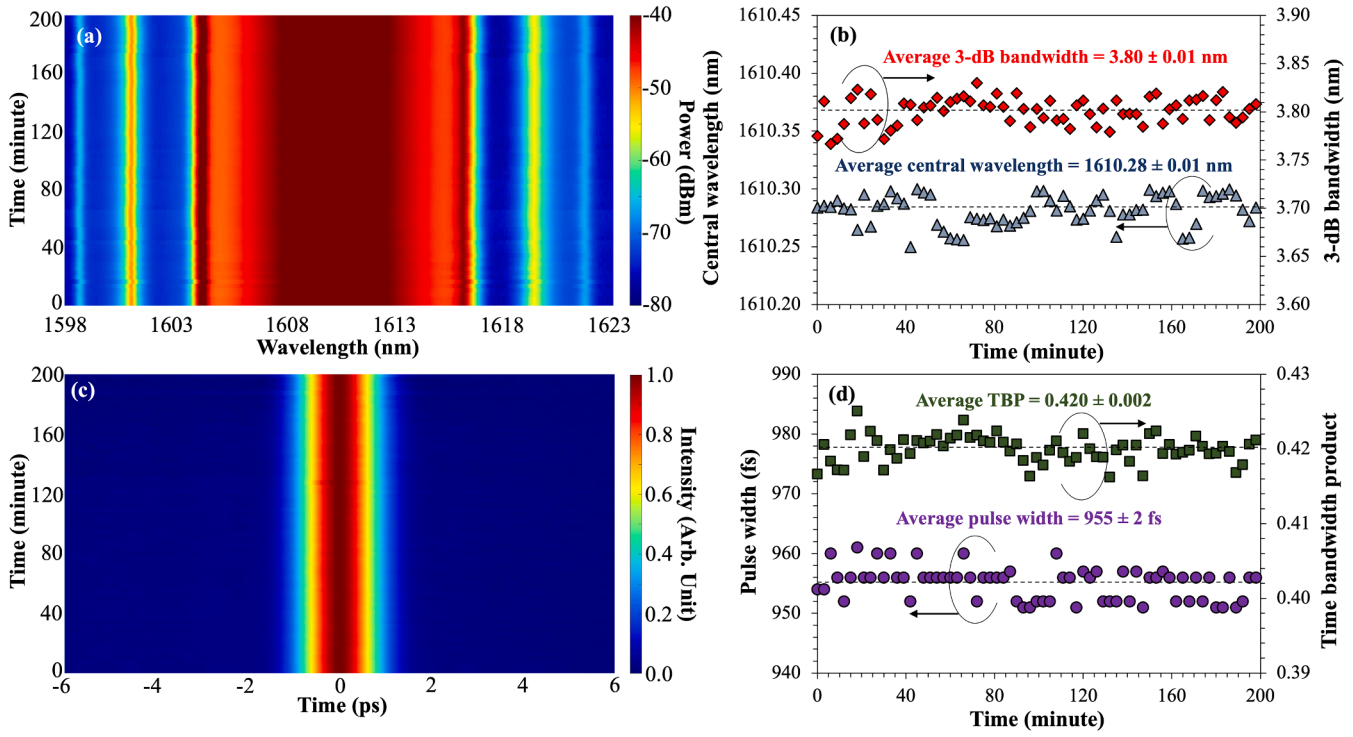

Fig.10. Stability evaluation of L-band mode-locked fiber laser over 200 min, (a) optical spectrum, (b) 3-dB bandwidth and central wavelength, (c) autocorrelation trace, and (d) TBP and pulse width.

Table 2
Review of mode-locked fiber laser for different metal oxides in C-band region.

Material	SA template	ΔT(%)	T_{ns} (%)	Power range (mW)	τ_{pulse}(fs)	P_{avg} (mW)	f_{rep} (MHz)	E_p (nJ)	Ref.
V_2O_5/PEO	FF	7.0	49.0	80.0–107.0	3140	4.72	1.00	4.44	[28]
CuO/PVA	FF	3.5	3.7	65.0–159.0	1700	1.27	0.98	1.29	[29]
Co_3O_4/PVA	FF	13.0	67.8	110.0–220.0	1240	11.72	5.68	1.99	[30]
Lu_2O_3/PVA	FF	10.0	58.0	145.0–187.0	2120	7.42	0.97	7.64	[31]
NiO/PEO	FF	39.0	49.0	100.0–165.0	950	1.09	0.96	1.14	[32]
Y_2O_3/PVA	FF	38.0	52.0	175.9–228.0	4150	25.48	1.01	25.80	[33]
VO_2	DSF	3.0	56.7	79.0–365.0	1280	7.83	22.91	0.34	[36]
TiO_{2-x}-MB	TF	7.1	51.9	40.0	978	–	9.93	–	[37]
Cr_2O_3	TF	12.5	67.5	580.0	334	–	34.48	–	[38]
NiO/PDMS	TF	4.0	61.5	50.0–250.0	793	7.14	8.07	0.89	[35]
γ-Al_2O_3/PDMS	TF	7.3	63.0	28.7–260.0	622	11.23	10.47	1.07	This work

*Note: FF: Fiber ferrule, DSF: D-shaped fiber, TF: tapered fiber, τ_{pulse}: pulse width, P_{avg}: Average output power, f_{rep}: repetition rate, E_p: pulse energy.

Table 3
Review of mode-locked fiber laser for different metal oxides in L-band region.

Material	SA template	λ_c (nm)	Power range (mW)	τ_{pulse} (fs)	P_{avg} (mW)	f_{rep} (MHz)	E_p (nJ)	Ref.
ZnO/PVA	FF	1599.50	42–159	2600	6.90	3.26	2.12	[39]
MgO/PVA	FF	1569.00	81–159	5600	7.60	3.50	2.17	[13]
H_2O_3/PVA	FF	1565.40	62–180	650	17.10	9.01	0.52	[40]
V_2O_5/PEG	FF	1596.00	80–107	1400	1.93	9.40	0.21	[34]
Fe_2O_3	FF	1572.39	100–225	4520	6.78	2.81	2.41	[11]
Fe_3O_4	TFG	1595.00	60–200	912	6.00	15.84	0.38	[41]
γ-Al_2O_3/PDMS	TF	1610.94	108.6–260	942	4.63	6.47	0.71	This work

*Note: FF: Fiber ferrule, TF: tapered fiber, λ_c: central wavelength, τ_{pulse}: pulse width, P_{avg}: Average output power, f_{rep}: repetition rate, E_p: pulse energy.

correspondingly. The oversaturation or slight damage to the SA device might be the main cause of these observations. Inversely, this work sustained the mode-locked operation until 260 mW pump power and remained stable during observation period without any CW breakthrough, pulse splitting effect or any sign of damage to the SA.

In other perspectives, Al-Hiti et al. integrated H_2O_3/PVA-SA into a 9.01 MHz laser cavity, delivering an ultrafast width of 650 fs and high output power of 17.10 mW, despite of very small output power extraction (5%). With comparable repetition rate, Baharom and co-workers reported a mode-locked operation utilizing V_2O_5/PEG-SA centered at near edge of L-band region (1596 nm) with slower pulse width of 1.4 ps [34]. This is stipulated to the lower rate of population inversion and

small net gain at longer wavelength in L-band which affect the rate of pulse amplification [42]. In the aspect of average output power, V_2O_5/PEG-SA had only 1.93 mW at 10% output port [34] whereas the output powers of Fe_3O_4/TFG-SA [41], ZnO/PVA-SA [39], MgO/PVA-SA [13] lie within 6.00 mW to 7.6 mW.

Besides that, at equivalent output splitting ratio of 20%, ferric oxide (Fe_2O_3)-SA [11] had slightly lower threshold mode-locked power and higher output power (100 mW, 6.78 mW) as compared to this work (108.6 mW, 4.63 mW). This is expected because the T_{ns} of our γ-Al_2O_3/PDMS-SA was at least 2.44 times larger than their work (65.0% vs. 26.7%) although the laser cavities were pumped at different power levels. Conversely, a moderate repetition rate of our laser cavity (6.47 MHz) produced the soliton pulse of 942 fs width, which was at least 4.8 times faster compared to the 2.81 MHz repetition rate of laser cavity incorporating Fe_2O_3-SA (4.52 ps) in Ref. [11]. Aside from that, the pulse energy attained by γ-Al_2O_3/PDMS-SA was measured to be 0.71 nJ, placing this work to be in between the reported works in Ref. [11,34,40,41] and Ref. [13,39].

Overall, the performances of C- and L-band of mode-locked pulses incorporating γ-Al_2O_3/PDMS-SA as pulse initiator were demonstrated and carefully discussed. Neither oversaturation nor sign of damage was observed throughout the experiments. This was made possible by exploiting weak evanescent wave interaction at the tapered fiber region, suggesting the damage threshold to be greater than input intensities of 8.49 GW/cm^2 and 3.57 GW/cm^2 in the C- and L-band regions, respectively. Furthermore, polymers like PVA and PEG are known for their hydrophilicity, which might be disadvantage to operate stably in high relative humidity environment, provided that their molecular weight are small. Conversely, PDMS offers high hydrophobicity and viscous characteristics that facilitate in encapsulating material and secure tapered fiber region from any mechanical breakage and environmental factors. In short, this work contributes to the femtosecond pulse generations of using metastable phase of Al_2O_3 that is beneficial for next generation of wideband photonic devices in the future.

Conclusion

This work has demonstrated γ-Al_2O_3/PDMS-SA as a promising candidate for photonic devices owing to its light absorbing properties. The optical fiber substrate for the fabricated SA was based on a tapered fiber, exhibiting 7.3% modulation depth and 303 MW/cm^2 saturation intensity at 1.56 μm wavelength. The device employment in the erbium-doped fiber laser cavities have successfully generated ultrafast pulses of 622 and 942 fs operating at 1.56 and 1.61 μm wavelengths, respectively. Marginal deviations in optical and time domains over 200 min observation period indicated stable mode-locked operations. The fabricated γ-Al_2O_3/PDMS-SA could withstand light intensities of greater than 8.49 and 3.57 GW/cm^2 in the C-band and L-band operations, respectively. Its robustness is due to the light-matter interaction of weak evanescent waves and also, the outstanding feature of dissipating heat longitudinally along the optical fiber. These research findings provide insightful information for future research on metastable state of aluminum-based materials for laser application in various photonic fields in near future.

Funding

This work was funded in part by the Ministry of Higher Education Malaysia under the Fundamental Research Grant Scheme (FRGS/1/2018/STG02/UPM/02/8) and the King Saud University, Kingdom of Saudi Arabia, under Researchers Supporting Project (RSP2024R336).

CRediT authorship contribution statement

N.F. Pikau: Writing – original draft, Visualization, Methodology, Investigation, Formal analysis, Conceptualization. **N. Mohd Yusoff:** Writing – review & editing, Supervision, Formal analysis. **A.R. Sarmani:** Supervision, Funding acquisition. **F.D. Muhammad:** Validation. **M.T. Alresheedi:** Funding acquisition. **E.K. Ng:** Resources. **M.A. Mahdi:** Writing – review & editing, Supervision, Project administration.

Declaration of competing interest

The authors declare that they have no known competing financial interests or personal relationships that could have appeared to influence the work reported in this paper.

Data availability

The data that has been used is confidential.

References

[1] Gemini L, Al-Bourgol S, Machinet G, Bakkali A, Faucon M, Kling R. Ablation of bone tissue by femtosecond laser: a path to high-resolution bone surgery. Materials 2021;14(9):2429. https://doi.org/10.3390/ma14092429.
[2] Shin S, Hur J, Park JK, Kim D. Thermal damage free material processing using femtosecond laser pulses for fabricating fine metal masks: influences of laser fluence and pulse repetition rate on processing quality. Opt Laser Technol 2021;134:106618. https://doi.org/10.1016/j.optlastec.2020.106618.
[3] Cai C, Wang J. Femtosecond laser-Fabricated photonic chips for optical communications: a review. Micromachines 2022;13(4):630. https://doi.org/10.3390/mi13040630.
[4] Bai R, Gao Y, Lu C, Tan J, Xuan F. Femtosecond laser micro-fabricated flexible sensor arrays for simultaneous mechanical and thermal stimuli detection. Measurement 2021;169:108348. https://doi.org/10.1016/j.measurement.2020.108348.
[5] Qin J, Dai R, Li Y, Meng Y, Xu Y, Zhu S, et al. 20 GHz actively mode-locked thulium fiber laser. Opt Express 2018;26(20):25769–77. https://doi.org/10.1364/oe.26.025769.
[6] Gluth A, Wang Y, Petrov V, Paajaste J, Suomalainen S, Härkönen A, et al. GaSb-based SESAM mode-locked Tm:YAG ceramic laser at 2 μm. Opt Express 2015;23(2):1361–9. https://doi.org/10.1364/oe.23.001361.
[7] Hua K, Wang DN, Chen Q. Passively mode-locked fiber laser based on graphene covered single-mode fiber with inner short waveguides. Opt Commun 2022;505:127520. https://doi.org/10.1016/j.optcom.2021.127520.
[8] Huang L, Zhang Y, Liu X. Dynamics of carbon nanotube-based mode-locking fiber lasers. Nanophotonics 2020;9(9):2731–61. https://doi.org/10.1515/nanoph-2020-0269.
[9] Wang T, Zhang W, Wang J, Wu J, Hou T, Ma P, et al. Bright/dark switchable mode-locked fiber laser based on black phosphorus. Opt Laser Technol 2020;123:105948. https://doi.org/10.1016/j.optlastec.2019.105948.
[10] Gao B, Li Y, Ma C, Shu Y, Wu G, Chen B, et al. Ta_4C_3 MXene as a saturable absorber for femtosecond mode-locked fiber lasers. J Alloy Compd 2022;900:163529. https://doi.org/10.1016/j.jallcom.2021.163529.
[11] Cheng P, Du Y, Han M, Shu X. Mode-locked and Q-switched mode-locked fiber laser based on a ferroferric-oxide nanoparticles saturable absorber. Opt Express 2020;28(9):13177–86. https://doi.org/10.1364/oe.391006.
[12] Al-Alani IAM, Ahmad BA, Ahmed MHM, Latiff AA, Al-Masoodi AHH, Lokman MQ, et al. Nanosecond mode-locked erbium doped fiber laser based on zinc oxide thin film saturable absorber. Indian J Phys 2018;93(1):93–9. https://doi.org/10.1007/s12648-018-1251-z.
[13] Khaleel WA, Sadeq SA, Al-Alani IAM, Ahmed MHM. Magnesium oxide (MgO) thin film as saturable absorber for passively mode locked erbium-doped fiber laser. Opt Laser Technol 2019;115:331–6. https://doi.org/10.1016/j.optlastec.2019.02.042.
[14] Alamouti AF, Nadafan M, Dehghani Z, Ara MHM, Vejdani-Noghreiyan A. Structural and optical coefficients investigation of γ-Al_2O_3 nanoparticles using Kramers-Kronig relations and Z–scan technique. J Asian Ceram Soc 2021;9(1):366–73. https://doi.org/10.1080/21870764.2020.1869881.
[15] Yang Z, Yang L, Wang P, Peng Z, Niu Y, Jiang W, Zhao F. Effect of sintering aid combined vacuum infiltration on the properties of Al_2O_3-based ceramics via binder jetting. Addit Manuf 2024;79:103898. https://doi.org/10.1016/j.addma.2023.103898.
[16] Schlacher J, Geier S, Schwentenwein M, Bermejo R. Towards 3D-printed alumina-based multi-material components with enhanced thermal shock resistance. J Eur Ceram Soc 2024;44(4):2294–303. https://doi.org/10.1016/j.jeurceramsoc.2023.11.009.
[17] Krella AK, Sobczyk AT, Krupa A, Jaworek A. Thermal resistance of Al_2O_3 coating produced by electrostatic spray deposition method. Mech Mater 2016;98:120–33. https://doi.org/10.1016/j.mechmat.2016.05.002.
[18] Zhang Y, Zu Y, He D, Liang J, Zhu L, Mei Y, et al. The tailored role of "defect" sites on γ-alumina: a key to yield an efficient methane dry reforming catalyst with superior nickel utilization. Appl Catal B 2022;315:121539. https://doi.org/10.1016/j.apcatb.2022.121539.
[19] Wang Z, Shen X, Jing M, Li C. Enhanced arsenic removal from drinking water by FeOOH/γ-Al_2O_3 granules. J Alloy Compd 2018;735:1620–8. https://doi.org/10.1016/j.jallcom.2017.11.284.

[20] Al-Hayali SKM, Mohammed DZ, Khaleel WA, Al-Janabi AH. Aluminum oxide nanoparticles as saturable absorber for C-band passively Q-switched fiber laser. Appl Opt 2017;56(16):4720–6. https://doi.org/10.1364/ao.56.004720.
[21] Muhammad AR, Zulkipli NF, Samsamnun FSM, Rosol AHA, Rusdi MFM, Khudus MIMA, et al. Q-switched induced by aluminium (III) oxide in erbium-doped fiber lasers. Journal Fotonik 2020;1(1):24–9. https://journalfotonik.com/index.php/jf/article/view/12.
[22] Al-Hayali SKM, Selleri S, Al-Janabi AH. Dual-wavelength passively Q-switched ytterbium-doped fiber laser based on aluminum oxide nanoparticle saturable absorbers. Chin Phys Lett 2017;34(11):114201. https://doi.org/10.1088/0256-307x/34/11/114201.
[23] Rizman ZI, Zulkipli NF, Arof H, Yasin M, Harun SW. Q-switched and tunable wavelength fiber laser utilizing nickel oxide saturable absorber and sagnac loop mirror filter. Infrared Phys Technol 2020;109:103433. https://doi.org/10.1016/j.infrared.2020.103433.
[24] Yusoff NM, Hadi MAW, Abidin NHZ, Alresheedi MT, Goh CS, Mahdi MA. Aluminum oxide/polydimethylsiloxane-based Q-switched mode-locked erbium-doped fiber laser. Optik 2022;257:168730. https://doi.org/10.1016/j.ijleo.2022.168730.
[25] Yusoff NM, Ahmed MHM, Ng EK, Alresheedi MT, Mayzan MZH, Mahdi MA. Noise-like pulse generation in 1.95 μm region using bulk α-alumina saturable absorber. Results Phys 2023;52:106843. https://doi.org/10.1016/j.rinp.2023.106843.
[26] Yuan X, Zhu J, Tang K, Cheng Y, Xu ZJ, Yang W. Formation and properties of 1-D alumina nanostructures prepared via a template-free thermal reaction. Procedia Eng 2015;102:602–9. https://doi.org/10.1016/j.proeng.2015.01.135.
[27] Salman AA, Al-Janabi AH. Aluminum nanoparticles saturable absorber as a passive Q-switcher for erbium-doped fiber laser ring cavity configuration. Laser Phys 2019;29(4):045102. https://doi.org/10.1088/1555-6611/ab02f8.
[28] Nady A, Baharom MF, Latiff AA, Harun SW. Mode-locked erbium-doped fiber laser using vanadium oxide as saturable absorber. Chin Phys Lett 2018;35(4):044204. https://doi.org/10.1088/0256-307x/35/4/044204.
[29] Sadeq SA, Harun SW, Al-Janabi A. Ultrashort pulse generation with an erbium-doped fiber laser ring cavity based on a copper oxide saturable absorber. Appl Opt 2018;57(18):5180–5. https://doi.org/10.1364/ao.57.005180.
[30] Yang Y, Yao Y, Wu Q, Wu C, Xu K, Xu X, et al. Co_3O_4 film saturable absorber for generating soliton mode-locked pulses in erbium-doped fiber laser. Opt Fiber Technol 2022;68:102808. https://doi.org/10.1016/j.yofte.2021.102808.
[31] Baharom MF, Rahman MFA, Latiff AA, Wang P, Harun SW. Lutetium (III) oxide film as passive mode locker device for erbium-doped fibre laser cavity. Opt Commun 2019;446:51–5. https://doi.org/10.1016/j.optcom.2019.04.047.
[32] Nady A, Ahmed MHM, Latiff AA, Ooi CHR, Harun SW. Femtoseconds soliton mode-locked erbium-doped fiber laser based on nickel oxide nanoparticle saturable absorber. Chin Opt Lett 2017;15(10):100602. https://doi.org/10.3788/col201715.100602.
[33] Zulkipli NF, Muhammad AR, Batumalay M, Rosol AHA, Altuncu A, Durak FE, et al. Yttrium oxide (Y_2O_3) as a pulse initiator in a mode-locking erbium-doped fiber laser. Photonics 2022;9(7):486. https://doi.org/10.3390/photonics9070486.
[34] Baharom MF, Rahman MFA, Latiff AA, Ahmad A, Jali MH, Harun SW. Passive mode locking erbium-doped fiber laser using V_2O_5 polyethylene glycol saturable absorber. Indonesian J Electr Eng Comput Sci 2023;32(1):269. https://doi.org/10.11591/ijeecs.v32.i1.pp269-275.
[35] Aziz SAC, Yusoff NM, Abidin NHZ, Abdullah CAC, Idris MI, Alresheedi MT, et al. Nickel oxide-embedded tapered fibre as a saturable absorber for ultrafast photonics. Optik 2023;295:171508. https://doi.org/10.1016/j.ijleo.2023.171508.
[36] Wang F, Qu Y, Lan D, Zhang X, Cheng T. VO2(M) nanoparticles saturable absorbers onto D-shaped fiber for mode-locked operation at 1560 nm band. Opt Laser Technol/Opt Laser Technol 2022;151:108060. https://doi.org/10.1016/j.optlastec.2022.108060.
[37] Lu X, Li S, Yan M, Chen J, Deng T, Nie G, et al. Organic dye-loaded reduced titanium dioxide as a broadband saturable absorber for ultrafast fiber lasers. RSC Adv 2024;14(17):11728–33. https://doi.org/10.1039/d3ra08925h.
[38] Li L, Cheng J, Zhao Q, Zhang J, Yang H, Zhang Y, et al. Chromium oxide film for Q-switched and mode-locked pulse generation. Opt Express 2023;31(10):16872–81. https://doi.org/10.1364/oe.491792.
[39] Alani IAM, Lokman MQ, Ahmed MHM, Al-Masoodi AHH, Latiff AA, Harun SW. A few-picosecond and high-peak-power passively mode-locked erbium-doped fibre laser based on zinc oxide polyvinyl alcohol film saturable absorber. Laser Phys 2018;28(7):075105. https://doi.org/10.1088/1555-6611/aabd24.
[40] Al-Hiti AS, Rahman MFA, Harun SW, Yupapin P, Yasin M. Holmium oxide thin film as a saturable absorber for generating Q-switched and mode-locked erbium-doped fiber lasers. Opt Fiber Technol 2019;52:101996. https://doi.org/10.1016/j.yofte.2019.101996.
[41] Wang H, Zhao F, Yan Z, Hu X, Zhou K, Zhang T, et al. Excessively tilted fiber grating based Fe_3O_4 saturable absorber for passively mode-locked fiber laser. Opt Express 2019;27(11):15693–700. https://doi.org/10.1364/oe.27.015693.
[42] Kuroda K, Sasahira K, Yoshikuni Y. Gain saturation of a CW-pumped erbium-doped fiber amplifier for nanosecond pulses. Opt Fiber Technol 2012;18(1):44–6. https://doi.org/10.1016/j.yofte.2011.11.005.